

CALIBRATING STELLAR VELOCITY DISPERSIONS BASED ON SPATIALLY-RESOLVED H -BAND SPECTRA FOR IMPROVING THE $M_{\text{BH}}-\sigma_*$ RELATION

WOL-RANG KANG¹, JONG-HAK WOO^{1,7}, ANDREAS SCHULZE², DOMINIK A. RIECHERS^{3,4}, SANG CHUL KIM⁵, DAESEONG PARK¹, AND VERNESA SMOLCIC⁶

¹Astronomy Program, Department of Physics and Astronomy, Seoul National University, 1 Gwanak-ro Gwanak-gu, Seoul, 151-742, Republic of Korea; woo@astro.snu.ac.kr

²Kavli Institute for Astronomy and Astrophysics, Peking University, 100871 Beijing, China

³Astronomy Department, Cornell University, 220 Space Science Building, Ithaca, NY 14853, USA

⁴Astronomy Department, California Institute of Technology, MC 249-17, 1200 East California Boulevard, Pasadena, CA 91125, USA

⁵Korea Astronomy and Space Science Institute, Daejeon 305-348, Republic of Korea and

⁶Physics Department, University of Zagreb, Bijenička cesta 32, 10002 Zagreb, Croatia

Draft version July 17, 2018

ABSTRACT

To calibrate stellar velocity dispersion measurements from optical and near-IR stellar lines, and to improve the black hole mass (M_{BH})- stellar velocity dispersion (σ_*) relation, we measure σ_* based on high quality H -band spectra for a sample of 31 nearby galaxies, for which dynamical M_{BH} is available in the literature. By comparing velocity dispersions measured from stellar lines in the H -band with those measured from optical stellar lines, we find no significant difference, suggesting that optical and near-IR stellar lines represent the same kinematics and that dust effect is negligible for early-type galaxies. Based on the spatially-resolved rotation and velocity dispersion measurements along the major axis of each galaxy, we find that a rotating stellar disk is present for 80% of galaxies in the sample. For galaxies with a rotation component, σ_* measured from a single aperture spectrum can vary by up to $\sim 20\%$, depending on the size of the adopted extraction aperture. To correct for the rotational broadening, we derive luminosity-weighted σ_* within the effective radius of each galaxy, providing uniformly measured velocity dispersions to improve the $M_{\text{BH}}-\sigma_*$ relation.

Subject headings: galaxies: kinematics and dynamics—galaxies: bulges—infrared: galaxies—techniques: spectroscopic

1. INTRODUCTION

The black hole mass (M_{BH}) correlation with host galaxy properties has been one of the main issues in understanding galaxy evolution and black hole growth. In particular, the relatively tight correlation between M_{BH} and stellar velocity dispersion ($M_{\text{BH}}-\sigma_*$) has been reported for nearby galaxies with dynamically measured M_{BH} (Ferrarese & Merritt 2000; Gebhardt et al. 2000a), as well as present-day active galaxies with M_{BH} determined from reverberation-mapping results (Onken et al. 2004; Woo et al. 2010). While early studies claimed a remarkably tight $M_{\text{BH}}-\sigma_*$ relation with its intrinsic scatter below ~ 0.3 dex (e.g., Tremaine et al. 2002), recent studies showed a larger intrinsic scatter and a steeper slope due to the increased sample size, inclusion of more diverse galaxies, i.e., late-type and pseudo bulge galaxies, and the improvements of M_{BH} measurements based on better dynamical modeling and data (Ferrarese & Ford 2005; Graham 2008; Gültekin et al. 2009a; McConnell et al. 2011, 2012).

In understanding BH-galaxy coevolution, the present-day $M_{\text{BH}}-\sigma_*$ relation sets a local calibration point as most observational studies investigated cosmic evolution of the $M_{\text{BH}}-\sigma_*$ relation by measuring an offset from the local relationship (e.g., Woo et al. 2006, 2008; Bennert et al. 2010, 2011b). At the same time, the present-day $M_{\text{BH}}-\sigma_*$ relation has been used for calibrating the M_{BH} of active galactic nuclei (AGN), which is determined from the kinematics of sub-pc scale broad-emission line region.

The unknown viral factor for converting the line-of-sight velocity of broad-line region gas to the intrinsic velocity, has been empirically determined by matching the $M_{\text{BH}}-\sigma_*$ relation of quiescent and active galaxies at $z \sim 0$ (Onken et al. 2004; Woo et al. 2010; Park et al. 2012). Thus, defining the $M_{\text{BH}}-\sigma_*$ relation in the local universe is of importance to unveil the nature of BH-galaxy coevolution.

Stellar kinematics studies based on the near-IR stellar lines became powerful as near-IR spectrographs combined with laser-guide star adaptive optics provides the best spatial resolution for the ground-based facilities (e.g., Watson et al. 2008). Moreover, measuring σ_* in the near-IR is more promising for AGN host galaxies since AGN-to-star flux ratios are much more favorable in the near-IR (Dasyra et al. 2007; Watson et al. 2008; Woo et al. 2010) while it is almost impossible to measure σ_* in the optical for host galaxies of high luminosity QSOs.

Despite the increasing usage of near-IR spectra for probing stellar kinematics, a proper comparison between optical and near-IR measurements is still lacking. By measuring velocity dispersion of 25 early-type galaxies based on the CO absorption band head at $2.29\mu\text{m}$ in the K -band, Silge & Gebhardt (2003) claimed that velocity dispersion measured from near-IR stellar lines was systematically smaller by 10-30% than that measured from optical stellar lines. In contrast, Rothberg & Fischer (2010) reported that optical and near-IR velocity dispersions were consistent for a sample of 23 early-type galaxies, by comparing σ_* measured from the CO band

⁷ Author to whom any correspondence should be addressed

heads in the K -band, with σ_* measured from the CaII triplet. Vanderbeke et al. (2011) also measured velocity dispersion based on the CO band heads for a sample of 22 early-type galaxies, and presented consistent results with respect to optical σ_* . The discrepancy among various studies may have resulted from the systematic uncertainties of the velocity dispersion measurements since the line dispersion was measured from intrinsically broad CO band heads in the K -band and template mismatch could be very strong (see Silge & Gebhardt 2003). In contrast, the H -band spectral range ($\sim 1.6\text{--}1.7\mu\text{m}$) contains many more stellar lines, e.g., Si I, CO, and Mg I than the K -band, and is possibly less susceptible to template mismatch although the presence of strong sky OH lines is a downside. To utilize the H -band stellar lines for studying stellar kinematics, a proper comparison is required between σ_* measured from H -band spectra with that measured from optical spectra stellar lines.

To derive reliable σ_* to represent the kinematics of the pressure-supported bulge or spheroidal component, the effect of the rotation component should be corrected for. In the case of galaxies with a rotating stellar disk, the line-of-sight velocity dispersion can be easily overestimated due to rotational broadening if a large aperture is used to extract a spectrum (e.g., Bennert et al. 2011a; Harris et al. 2012). The effect of rotational broadening is stronger for more edge-on stellar disks, potentially producing systematic bias. Thus, it is important to correct for rotational broadening.

In this paper, we measure the stellar velocity dispersion of 31 nearby galaxies using high quality H -band spectra. We compare σ_* measurements based on stellar lines in the H -band with optical σ_* measurements from the literature. We also correct for the rotation and aperture effect based on the spatially resolved kinematics measurements to improve the $M_{\text{BH}}\text{--}\sigma_*$ relation. The paper is organized as follows. We describe sample selection, observations and data reduction in § 2. In § 3, we present σ_* measurements, and the effects of rotation and aperture size. In § 4, we compare our H -band σ_* measurements with optical σ_* from the literature, and derive the $M_{\text{BH}}\text{--}\sigma_*$ relation for early-type galaxies based on the rotation-corrected σ_* . The main results are summarized in § 5.

2. OBSERVATIONS AND DATA REDUCTION

2.1. Sample Selection and Observations

To directly compare optical and near-IR stellar velocity dispersions and to calibrate the $M_{\text{BH}}\text{--}\sigma_*$ relation, we select 31 nearby galaxies from the $M_{\text{BH}}\text{--}\sigma_*$ sample (e.g., Gültekin et al. 2009a), for which dynamical M_{BH} measurements and optical σ_* measurements are available. The sample is mainly composed of early-type galaxies (20 ellipticals, 8 lenticulars and 3 spirals) and spans a wide range in σ_* from 67 km s^{-1} to 385 km s^{-1} as listed in Table 1. Also, it covers three orders of magnitude in M_{BH} and constitutes about half the sample size of galaxies with dynamical M_{BH} measurements (McConnell & Ma 2013).

Observations were performed at the Palomar Hale 5 m telescope using the near-IR spectrograph TripleSpec, simultaneously covering the wavelength range from $1.0\mu\text{m}$ to $2.4\mu\text{m}$. In this work we only employ the H -band spec-

tra centered at $\sim 1.7\mu\text{m}$, as it covers many stellar absorption lines suitable for the σ_* measurement. We place an $1'' \times 30''$ long-slit along the major axis of each galaxy. The spectral resolution of TripleSpec is $R = 2500 - 2700$, corresponding to a Gaussian dispersion $\sim 50\text{ km s}^{-1}$. As the lowest optical σ_* is 67 km s^{-1} (for NGC 7457), this spectral resolution is suitable for our study.

For sky subtraction, in particular for the strong OH sky emission lines, we also observed blank sky, offset by several arc minutes from each galaxy, since the size of each galaxy is larger than the slit length and fills the entire slit. We divide the total exposure time into segments of 200 second exposures to avoid saturation in the K -band. The total on-source exposure time ranges from 600 to 1000 seconds depending on the magnitude of individual galaxies (see Table 1). We observed several A0V stars each night to correct for telluric lines. We also observed 11 K- and M-type giant stars as velocity templates for the stellar velocity dispersion determination.

2.2. Data Reduction

We performed standard data reduction, i.e., bias subtraction, flat-fielding and wavelength calibration using a series of IRAF scripts, then extracted one-dimensional spectra using various extraction windows. For telluric absorption correction, we constructed a telluric line template for each observing night, based on the spectra of A0V stars observed during the night. For each A0V star, we fitted their Brackett lines with double Gaussians and normalized the spectra by its continuum. Dividing the observed A0V star spectrum by this model spectrum provides a telluric template. We combined all telluric templates to construct a mean template for a given night. Then, we used the template to correct the galaxy spectra for telluric absorption lines.

To investigate the effect of galaxy rotation on stellar velocity dispersion measurements, we extracted spatially resolved spectra from a number of small extraction windows (4-16 pixels) along the galaxy's major axis, which were allowed to overlap with each other and to slightly increase at larger radii for obtaining better signal-to-noise. The resolution for spatial binning depends on the distance to each galaxy. Typically ~ 10 spectra were extracted within a fraction of the R_e (see Section 3.5 for details).

A series of single-aperture spectra were also extracted using various aperture sizes, in order to investigate the aperture effect. Many previous studies used spatially unresolved σ_* measurements, which were affected by line broadening due to galaxy rotation. This leads to an overestimation of the galaxy's σ_* , depending on how much rotation is included in the extraction aperture. Thus, the choice of different aperture sizes can affect the σ_* measurement as presented in § 3.4. In contrast, we can correct the σ_* measurement for the rotational broadening using our spatially resolved spectra. Details on this correction are presented in § 3.4 and § 3.5.

3. ANALYSIS

3.1. Stellar Velocity Dispersion Measurements

We measured the stellar velocity dispersion of 31 galaxies in the sample using the stellar lines in the $1.57 - 1.72\mu\text{m}$ range, i.e., CO(4-1) $1.58\mu\text{m}$ Si I $1.59\mu\text{m}$ CO(5-

TABLE 1
SAMPLE SELECTION AND OBSERVING LOG

Galaxy	RA (J2000)	DEC (J2000)	Type	Dist. (Mpc)	Spatial Scale (kpc/1'')	R_e (kpc)	Ref.	M_{BH} ($10^8 M_{\odot}$)	Ref.	UT Date	T_{EXP} (s)	S/N	PA ($^{\circ}$)
(1)	(2)	(3)	(4)	(5)	(6)	(7)	(8)	(9)	(10)	(11)	(12)	(13)	(14)
N221	00 42 41.87	+40 51 57.2	E2	0.86	0.0037	0.24	1	0.026±0.005	25, 6	10 Jan 1	600	414	170
N821	02 08 21.04	+10 59 41.1	E4	25.5	0.1202	15.7	2	1.7±0.7	25, 7	10 Jan 1	600	133	25
N1023	02 40 23.90	+39 03 46.3	SB0	12.1	0.0442	1.1	2	0.4±0.04	25, 8	10 Jan 1	600	320	87
N1068	02 42 40.83	-00 00 48.4	Sb	15.4	0.0788	2.9	2	0.086±0.003	5, 9	10 Jan 1	600	455	13
N2778	09 12 24.35	+35 01 39.4	E2	24.2	0.1420	3.0	1	0.16 ^{+0.09} _{-0.102}	4	09 May 22	600	158	40
N2787	09 19 18.90	+69 12 11.9	SB0	7.9	0.0482	0.27	2	0.41 ^{+0.04} _{-0.05}	25, 10	09 May 25	600	247	109
N3031	09 55 33.17	+69 03 55.1	Sb	4.1	0.0179	3.0	2	0.8 ^{+0.2} _{-0.11}	25, 11	10 Jan 1	600	393	149
N3115	10 05 13.80	-07 43 08.0	S0	10.2	0.0460	2.9	2	8.9 ^{+5.1} _{-2.7}	25, 12	10 Jan 1	600	362	40
N3245	10 27 18.52	+28 30 24.8	S0	22.1	0.0911	1.0	2	2.1 ^{+0.5} _{-0.6}	25, 13	09 May 22	600	247	177
N3377	10 47 42.36	+13 59 08.8	E6	11.7	0.0461	3.9	2	1.8±0.9	25, 7	10 Jan 1	600	244	41
N3379	10 47 49.75	+12 34 54.6	E0	11.7	0.0631	2.7	2	4.2 ^{+1.0} _{-1.1}	25, 14	09 May 22	600	307	73
N3384	10 48 16.90	+12 37 42.9	SB0	11.7	0.0488	0.48	2	0.11±0.05	25, 7	10 Jan 1	600	254	53
N3607	16 12 54.64	+18 03 06.3	E1	19.9	0.0665	4.3	3	1.4 ^{+0.4} _{-0.5}	25, 12	10 Jan 1	800	229	125
N3608	11 16 59.07	+18 08 54.6	E1	23.0	0.0869	3.9	2	4.7±1.0	25, 7	09 May 25	800	252	75
N4258	12 18 57.54	+47 18 14.3	SABbc	7.2	0.0310	0.66	2	0.367±0.001	25, 16	09 Mar 5	600	229	150
N4261	12 19 23.21	+05 49 29.7	E2	33.4	0.1551	5.8	2	5.3±1.1	25, 17	09 May 25	600	203	160
N4291	12 20 17.60	+75 22 15.0	E2	25.0	0.1218	2.0	2	9.8±3.1	25, 7	10 Jan 1	800	164	110
N4342	12 23 39.12	+07 03 12.9	S0	18.0	0.0520	0.21	2	4.6 ^{+2.6} _{-1.0}	25, 18	09 Mar 5	800	104	168
N4374	12 25 03.74	+12 53 13.1	E1	17.0	0.0735	7.8	2	9.2 ^{+1.0} _{-0.8}	25, 19	10 Jan 1	600	250	122.5
N4459	12 29 00.13	+13 58 42.5	E2	17.0	0.0839	13.7	2	0.7 ^{+0.13} _{-0.14}	25, 10	09 Mar 5	600	206	110
N4473	12 29 48.95	+13 25 46.1	E4	17.0	0.1555	2.1	2	0.89 ^{+0.45} _{-0.44}	25, 7	09 Mar 5	600	170	100
N4486	12 30 49.42	+12 23 28.0	E1	17.0	0.0906	6.0	2	62.0 ^{+3.0} _{-4.0}	25, 20	09 May 22	600	168	153
N4564	12 36 27.01	+11 26 18.8	S0	17.0	0.0791	3.0	1	0.88±0.24	25, 7	09 May 25	600	272	47
N4596	12 39 56.16	+10 10 32.4	SB0	18.0	0.1296	1.5	2	0.84 ^{+0.36} _{-0.25}	25, 10	09 May 25	600	208	75
N4649	12 43 40.19	+11 33 08.9	E2	16.5	0.0774	7.2	2	47.0 ^{+11.0} _{-10.0}	25, 21	09 May 22	600	221	105
N4697	12 48 35.70	-05 48 03.0	E6	12.4	0.0860	6.9	2	2.0±0.2	25, 7	10 Jan 1	600	260	70
N4742	12 51 47.92	-10 27 17.1	E4	16.4	0.0880	1.6	2	0.14±0.05	24	09 May 25	600	355	75
N5845	15 06 00.90	+01 38 01.4	E3	28.7	0.1005	0.42	2	4.9 ^{+1.5} _{-1.6}	25, 7	09 May 22	600	274	141
N6251	16 32 31.97	+82 32 16.4	E1	106.0	0.5134	10.0	2	6.0±2.0	25, 22	09 May 22	600	141	21
N7052	21 18 33.13	+26 26 48.7	E3	70.9	0.3238	9.1	2	4.0 ^{+2.8} _{-1.6}	25, 23	09 May 25	1000	185	62
N7457	23 01 00.05	+30 08 43.4	S0	14.0	0.0563	4.8	1	0.10±0.06	5, 7	09 May 25	600	131	125

NOTE. — Col. (1): NGC galaxy catalogue name. Col. (2) Right Ascension. Col. (3): Declination. Col. (4): morphological types. Col. (5): distance. Col. (6): spatial scale. Col. (7)-(8): effective radius and reference. Col. (9)-(10): black hole mass and their reference. Col. (11): observation date. Col. (12): total exposure time. Col. (13): average signal-to-noise ratio within ± 5 pixel aperture. Col. (14): Position Angle. References. — (1) Marconi & Hunt (2003); (2) Graham (2008); (3) Sani et al. (2011); (4) Gültekin et al. (2009a); (5) McConnell et al. (2011); (6) Verolme et al. (2002) (7) Schulze & Gebhardt (2011); (8) Bower et al. (2001); (9) Lodato & Bertin (2003); (10) Sarzi et al. (2001); (11) Devereux et al. (2003); (12) Emsellem, Dejonghe & Bacon (1999); (13) Barth et al. (2001); (14) van den Bosch & de Zeeuw (2010); (15) Gültekin et al. (2009b); (16) Herrnstein et al. (2005); (17) Ferrarese, Ford & Jaffe (1996); (18) Cretton & van den Bosch (1999); (19) Walsh, Barth & Sarzi (2010); (20) Gebhardt et al. (2011); (21) Shen & Gebhardt (2010); (22) Ferrarese & Ford (1999); (23) van der Marel & van den Bosch (1998); (24) Tremaine et al. (2002); (25) McConnell & Ma (2013)

2) $1.6\mu\text{m}$ CO(6-3) $1.62\mu\text{m}$ CO(7-4) $1.64\mu\text{m}$ CO(8-5) $1.66\mu\text{m}$, and Mg I $1.71\mu\text{m}$ (see Figure 1). Using the Gauss-Hermite Pixel Fitting software (van der Marel 1994; Woo et al. 2004, 2005, 2006), we performed χ^2 minimization in fitting the galaxy spectra directly in pixel space to stellar template spectra broadened by a Gaussian kernel with velocity widths ranging from 50 to 350 km s^{-1} . The continua of the spectra of the template stars are fitted with low-order (2-3) polynomials while the FeII emission line at $1.65\mu\text{m}$, bad pixels and residuals from sky line subtraction were masked out before the fitting.

3.2. Template Mismatch

Since the σ_* measurement is affected by the choice of template star, it is necessary to quantify the uncertainty due to the template mismatch. Using 11 velocity template stars of various spectral types, namely, K0 III, K1

III, K2 III, K5III, two M0 III, M1 III, two M2 III, M3 III, and M5 III, which were observed with the same instrumental setup during our observing runs, we measured and compared σ_* for individual galaxies in the sample, in order to investigate the variation in the σ_* measurement caused by template mismatch. Then, we accounted for template mismatch in the determination of σ_* by averaging σ_* measurements using various template stars.

To compare the overall spectral shapes, we present the spectra of the individual template stars, after broadening them with a Gaussian velocity (red thick lines) in Figure 1. The observed spectrum of NGC 1023 is overplotted (black lines) to demonstrate the template mismatch. In the stellar spectra, the line strength of the CO absorption lines increases toward later-type stars (from upper panels to lower panels). This trend is in particular clearly shown for the CO(6-3) line at $1.62\mu\text{m}$ and also for the MgI line at $1.71\mu\text{m}$. On the other hand, the SiII line strength

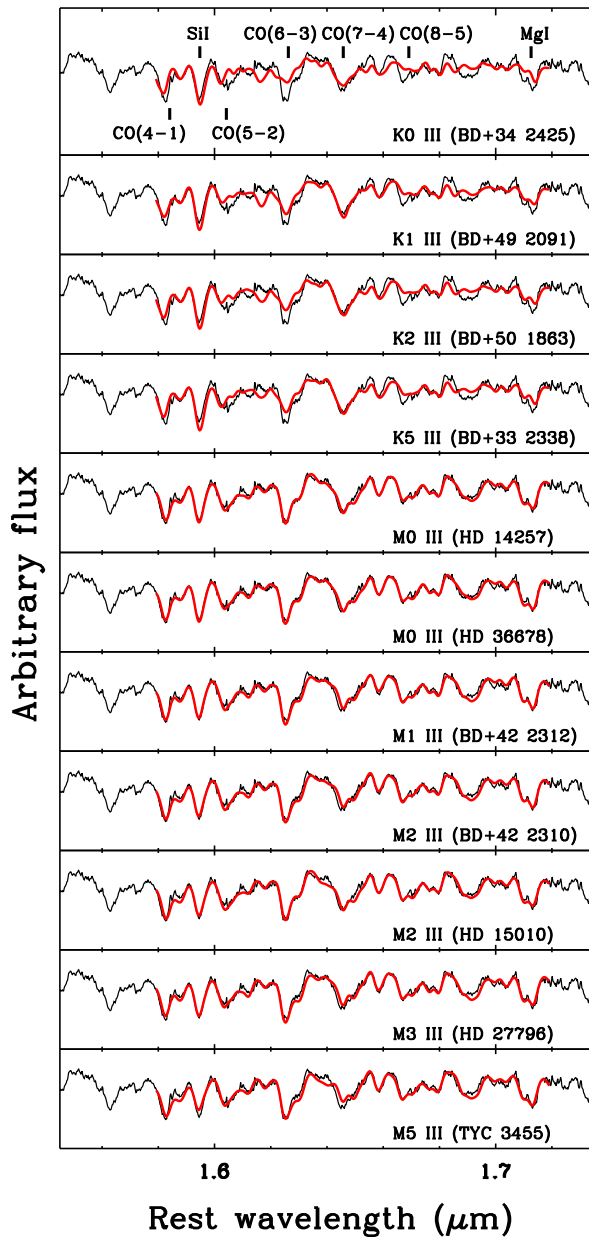


FIG. 1.— Normalized spectra of template stars. The template star spectra (thick red solid line) are compared with the spectra of NGC 1023 (thin black solid line). The template star is broadened with a Gaussian velocity kernel. Individual template stars show different line strengths, particularly for the CO absorption line. The K type star templates provide a poor fit to the galaxy spectrum. In the top panel, we marked several individual stellar lines with black tick masks (from left, CO(4-1), SiI, CO(5-2), CO(6-3), CO(7-4), CO(8-5) and MgI).

shows no strong variation with spectral type. The comparison in Fig. 2 clearly shows that spectra of K type stars provide a poor match to the observed galaxy spectrum in this wavelength range, while spectra of M type stars can fit the observed galaxy spectrum reasonably well.

In Figure 2, we compare the multiple measurements of σ_* of NGC 1023, using each template star for the fitting. As expected from Figure 1, the σ_* measured from M-

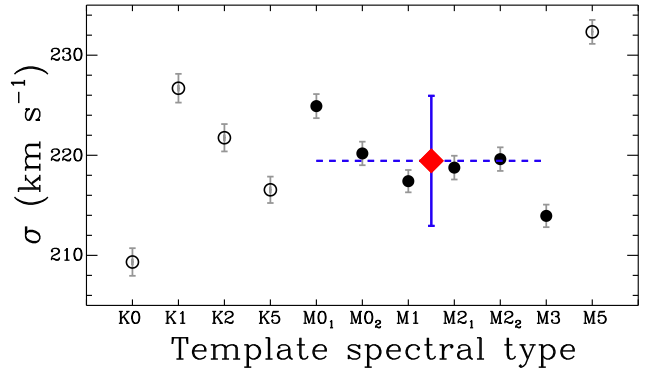


FIG. 2.— Comparison of the measured stellar velocity dispersion of NGC 1023 using different template stars. Filled circles denote M0 III, M1 III, M2 III and M3 III type stars, which were used for calculating the mean stellar velocity dispersion. Open circles denote M5 III and K type template stars. The mean σ_* is given by the red diamond and the standard deviation of the measurements is included in the uncertainty denoted by the blue solid error bar. The blue dashed line indicates the range of template stars used for calculating the mean stellar velocity dispersion.

type stars shows small variation, while σ_* measured from K-type stars exhibits a larger scatter, suggesting that M-type stars provide a fair representation of the luminosity-weighted stellar population in the H -band. Therefore, we excluded the measurements from K-type stars and calculated the mean σ_* based on the 6 M-type stars. Since the M5 III star shows slightly different line shapes compared to other M-type stars (see Figure 1), we also excluded the measurement based on the M5 III template. After calculating the standard deviation of the measurements from 6 M-type stars as the uncertainty of template mismatch, we added the uncertainty of template mismatch to the mean measurement errors from 6 M-type stars in quadrature, in order to determine the uncertainty of σ_* . For example, the red diamond in Figure 2 indicates the mean σ_* , derived from 6 template stars and its uncertainty. In Figure 3, we present the normalized observed spectrum (black solid line) of each galaxy in the sample, overplotted with the best-fit model (red solid line).

3.3. Spatially Resolved Stellar Velocity Dispersions

By extracting spectra over several bins along the major axis, we obtained spatially resolved kinematics. In Figures 4 and 5 we show the radial profiles of line-of-sight velocities (upper panel) and velocity dispersions (lower panel) for each galaxy. We used the line-of-sight velocity of the galaxy center as a reference and normalized all velocities with respect to the central value. For most galaxies we extracted 9-13 spectra along the slit (in the direction of the major axis) out to $\pm 7''$ from the center. This is smaller than the slit size ($\pm 15''$) since we were not able to use outer pixels due to much lower S/N than the central bins to measure σ_* and the ABBA dither pattern along the slit.

Among the sample galaxies, we find a clear rotation component for 25 out of 31 objects. The amplitude of the projected rotation velocity ranges from $\sim 40 \text{ km s}^{-1}$ to over 200 km s^{-1} while six galaxies, namely NGC 1068, NGC 3608, NGC 4261, NGC 4374, NGC 4486 and NGC 6251 show a weak or no rotation component. For the galaxies with a significant rotation component, we expect

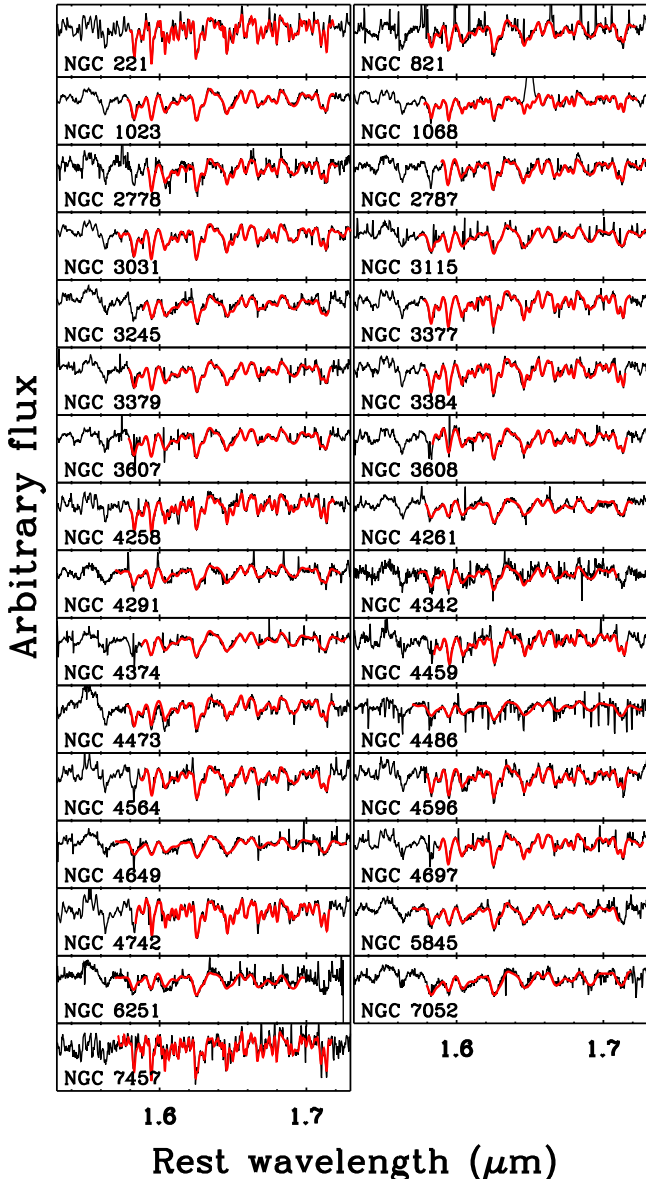


FIG. 3.— Normalized spectra of the 31 galaxies and their best-fit models. The broadened template star spectra (thick red solid line) fit the observed galaxy spectra (thin black solid line) reasonably well. Residuals of OH sky emission lines (sharp features in Fig. 1) and the AGN Fe II emission line (e.g., in NGC 1068) were masked out before fitting.

line broadening due to the rotation, leading to overestimation of σ_* , if a large single aperture is used for extraction. While the magnitude of this effect depends on the details of radial profiles of rotation and velocity dispersion of each galaxy, it will lead to a systematic bias if not taken into account. We will account for the rotation component in the stellar velocity dispersion measurement in the next subsection.

In the lower panels of Figure 4 and Figure 5, we show the stellar velocity dispersion profiles along the major axis. While stellar velocity dispersion decreases from the center to the outer regions for most galaxies, several galaxies, e.g., NGC 1068, NGC 4261, NGC 4374, NGC 4596 and NGC 7052, do not show such a decrease-

ing trend of σ_* , but rather show irregular shapes; flat, increasing or asymmetric trends as similarly reported by previous studies based on optical kinematics studies (e.g. Dressler 1984; Bender, Saglia & Gerhard 1994; Kent 1990; Pinkney et al. 2003).

3.4. Aperture Size Effect

We investigate the effect of using different aperture sizes on the measured stellar velocity dispersion, by directly measuring σ_* from apertures of increasing size. In Figure 6 we present the σ_* measurements as a function of aperture size, after normalizing them to the σ_* measured from the smallest aperture (4-10"). We find three different trends (increasing, flat and decreasing) of σ_* with increasing aperture size. The 8 galaxies shown in the upper panels exhibit an increase of σ_* as a larger aperture size is used, while for 13 galaxies shown in the lower panels, σ_* decreases with increasing aperture size. These galaxies show variation of σ_* up to 20% as aperture size changes. In contrast, 10 galaxies (middle panels) do not show clear change of σ_* as a function of aperture size.

Thus, when measuring σ_* from a large aperture it is possible to either overestimate or underestimate σ_* . The magnitude and direction of this bias depends on two factors: (1) the overestimation caused by rotational line broadening and (2) the natural decrease of σ_* as a function of radius. The galaxies in the upper panels in Figure 6 are dominated by the first effect. They show relatively strong galaxy rotation and only a mild decrease in their velocity dispersion profile, as shown in Figures 4 and 5, leading to a net increase in σ_* with increasing aperture size. For these galaxies, when the extraction aperture covers outer parts of the galaxy, where the rotation curves flatten, the aperture effect on σ_* also flattens. This is clearly seen for example in the case of NGC 3384, which shows a flattening of σ_* beyond the third bin, corresponding to the flattening of the rotation curve in Figure 4. NGC 4742 even shows a decrease in σ_* beyond the radius where the rotation curves becomes flat.

The decreasing σ_* trend for the galaxies in the lower panels of Figure 6 can be explained in a similar way. For these galaxies the decrease in σ_* profile is dominating over line broadening due to rotation. For example, NGC 4486 shows the largest variation in σ_* as a function of aperture size since it has no significant rotation component while the velocity dispersion profile is strongly decreasing toward larger radii. Similarly, NGC 3608 and NGC 4649 also show strong decrease, which is dominated by the strong decrease in σ_* with radius. In contrast, there are galaxies, e.g., NGC 821, where the effect from the rotation curve and the decreasing σ_* profile are roughly of the same order, leading to a small net variation of σ_* measured from different apertures.

3.5. Correction of the Galaxy Rotation Effect

As discussed above, σ_* measured within a certain aperture will be susceptible to line broadening by galaxy rotation. In contrast, the spatially resolved stellar velocity dispersions, represented in Figure 4 and Figure 5, do not suffer rotational broadening. Thus, we can use these measurements to compute a rotation-corrected σ_* . We

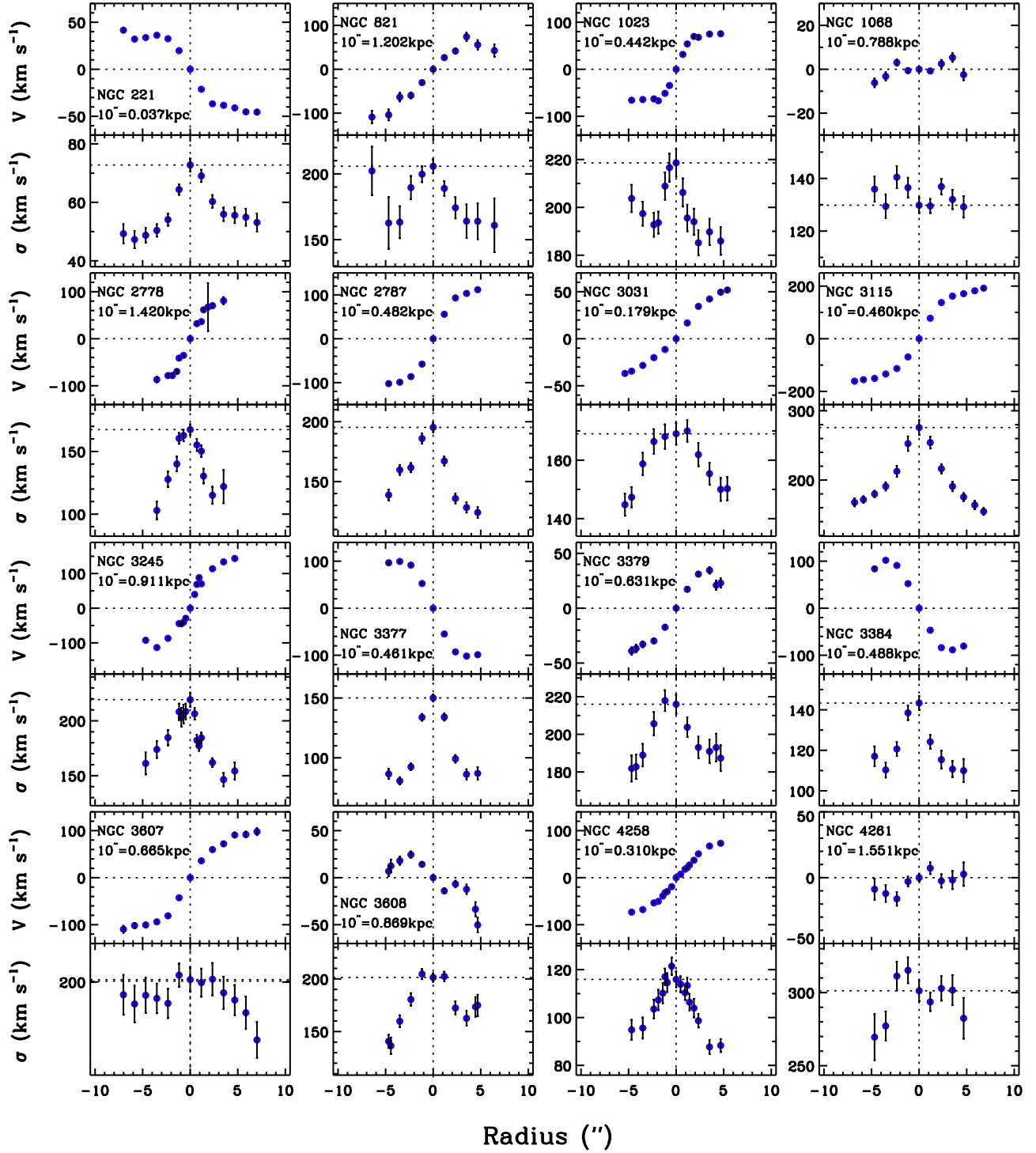


FIG. 4.— The line-of-sight velocities (upper panel) and stellar velocity dispersions (lower panel) along the major axis. Most galaxies show a clear rotation component and a radial decrease of σ_* . The object name and the spatial scale are shown in each upper panel.

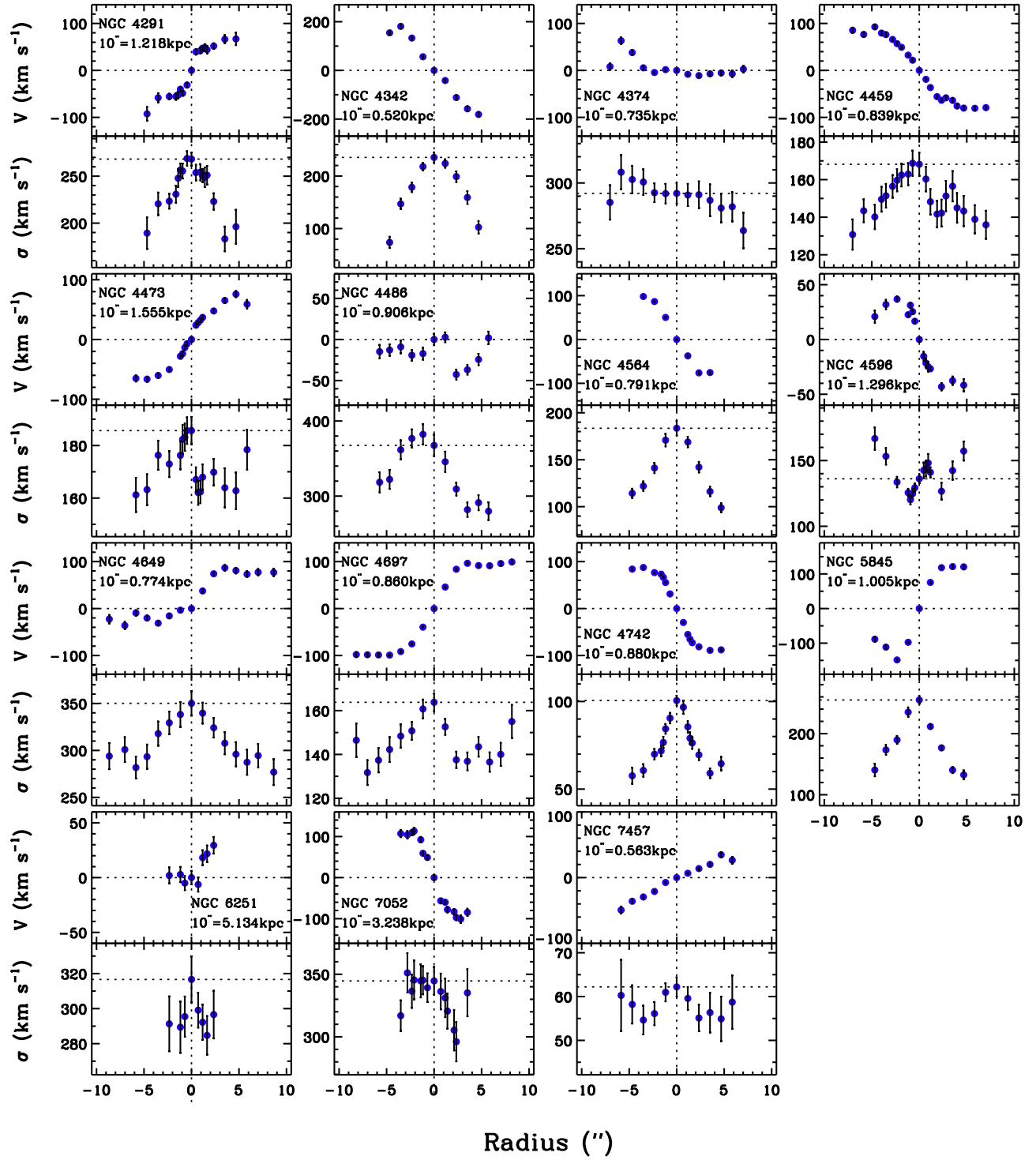


FIG. 5.— Same as Figure 4 for the rest of the sample.

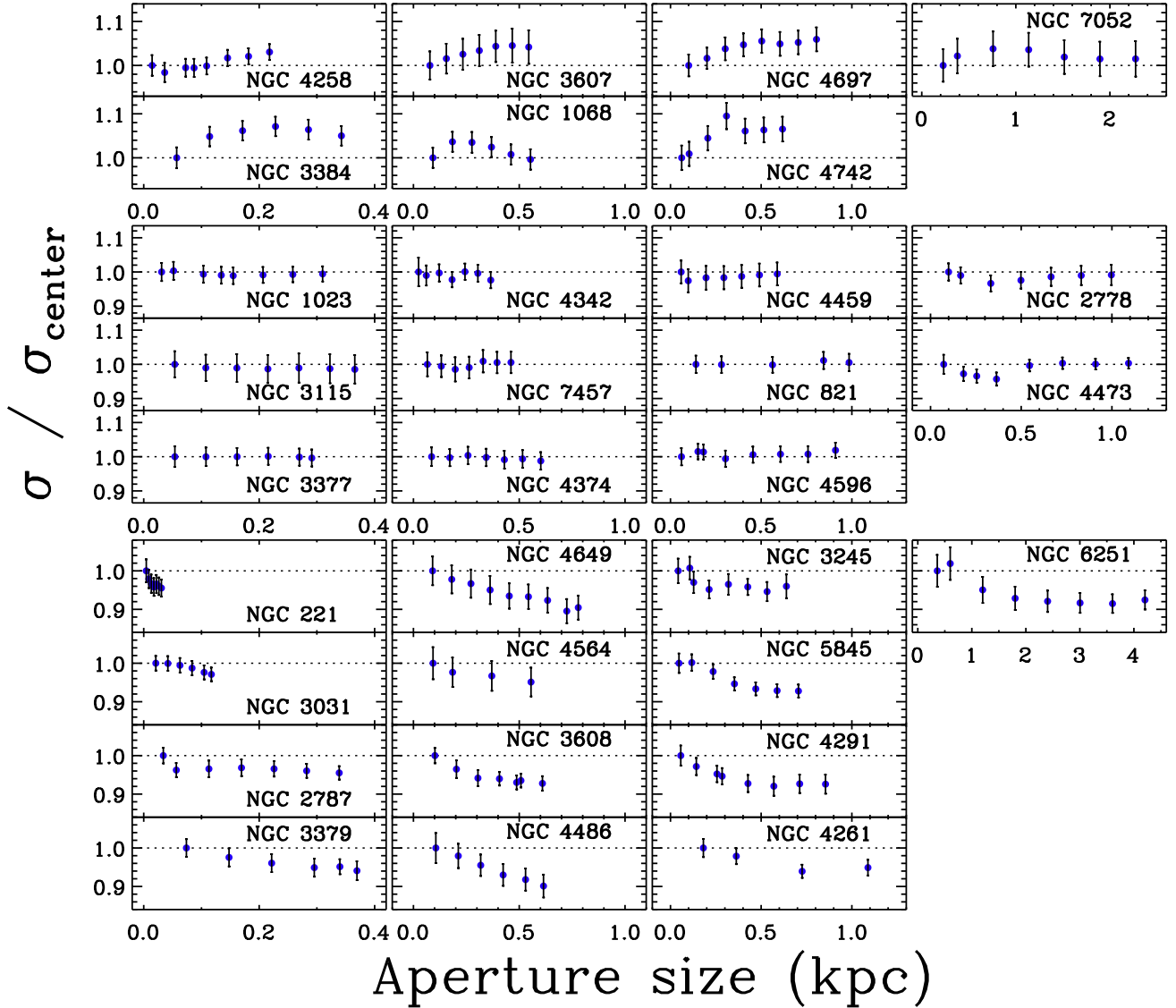


FIG. 6.— Stellar velocity dispersions measured from various aperture sizes. Each σ_* measurement is normalized by σ_* measured from the smallest aperture. Upper panels show the objects that have increasing trend while Lower panels show the objects with an opposite trend. Middle panels show the objects that have constant trend of σ_* . Galaxies are sorted by the distance.

compute luminosity-weighted σ_* within a radius R :

$$\sigma_R = \frac{\int_{-R}^R \sigma_*(r) I(r) dr}{\int_{-R}^R I(r) dr} \quad (1)$$

where $I(r)$ is the surface brightness profile of the galaxy and R is the outer radius within which we compute σ_* . Using the spectral images, we measure the surface brightness profile of each galaxy by fitting with two Gaussian models, and use this fit to compute the luminosity-weight for the σ_* measured at each radius. We chose an outer radius R for each galaxy based on the R_e (see Table 1). For 20 galaxies, we were able to measure spatially resolved σ_* only at the central parts, due to the limited spatial coverage and/or lower S/N at the outer part. Thus, we chose $1/8$ of R_e as an outer radius in Eq. 1. For the other 11 galaxies, we measured σ_* over a

larger fraction of R_e ($1/4$ to unity) as an outer radius and corrected for the rotation component as listed in Table 2.

In Figure 7 we illustrate the effect of the correction for galaxy rotation. Here, σ_R is the luminosity-weighted σ_* within R as computed from Equation 1 while $\sigma_R(\text{uncor})$ is measured from a single aperture with an aperture size of R . As expected, most galaxies show a decrease in velocity dispersion when accounting for the rotation component while for galaxies without strong rotation component, the correction is marginal. Including 6 galaxies that show no rotation, the average correction is 6%, while the correction for individual galaxies can be up to $\sim 20\%$. The magnitude of the rotation correction tends to be smaller for more massive galaxies. NGC 7052 with the highest σ_* in the sample seems to be an outlier from this trend since it has relatively large rotation while σ_* mildly decreases within $R_e/8$. In summary, we find

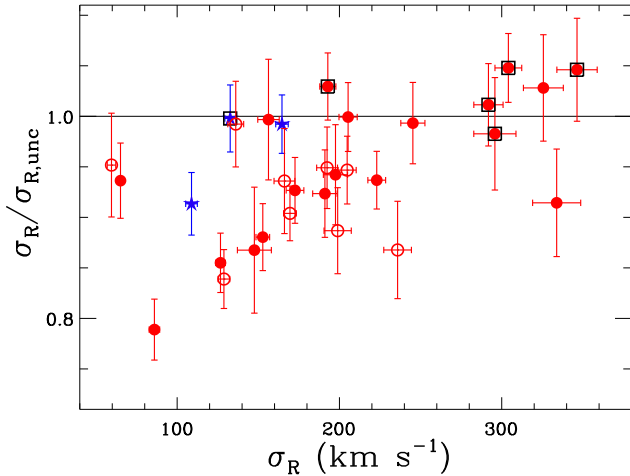


FIG. 7.— Ratio of velocity dispersions determined with and without rotation correction as a function of velocity dispersion. Filled and open circles represent elliptical and lenticular galaxies, respectively, while stars denote late-type galaxies. Six galaxies without a clear rotation component are marked with open squares.

that stellar velocity dispersions measured from single-aperture spectra can be biased by up to $\sim 20\%$. This is consistent with the results of Bennert et al. (2011a) and Harris et al. (2012).

A possible drawback for the comparison with previous studies, that usually report σ_* measured within R_e , is the limited spatial coverage in our work, restricting our measurements to $R_e/8$. To investigate the effect on the σ_* measurement, we tested two extreme cases. First, we assumed a constant σ_* from $R_e/8$ to R_e , equal to the value at $R_e/8$. Second, we extrapolated the decreasing stellar velocity dispersion profile out to R_e . For both cases we computed the luminosity-weighted σ_* within R_e via Equation 1. We found that σ_* values decrease by only a few per cent by increasing the outer radius from $R_e/8$ to R_e in both cases, due to the much lower luminosity weight at outer radii. Thus, our σ_* measurements within $R_e/8$ will closely resemble the value that would be measured at R_e .

4. DISCUSSION

4.1. Optical vs. near-IR Velocity Dispersions

In Figure 8 we compare the stellar velocity dispersions measured using our near-IR spectra (σ_{IR}) with the literature values measured from optical spectra (σ_{opt}). For this comparison, we collected σ_{opt} measurements from McConnell & Ma (2013), who listed their own measurements as well as previously measured values from the literature (see Table 2). Although these optical measurements were based on spatially resolved stellar kinematics and the quoted values were luminosity-weighted or averaged velocity dispersions within the R_e for most galaxies, these values were not homogeneously measured due to the various data quality and the measurement methods. In addition, some of these values in the original works were measured with a smaller aperture size than R_e or the aperture size was not clearly stated for many cases in the original references.

Thus, we decide to compare both H -band σ_* measurements with/without rotation correction to the optical σ_* measurements. As shown in Figure 8, we find no sig-

TABLE 2
NEAR-IR AND OPTICAL STELLAR VELOCITY DISPERSIONS

Name (1)	σ_{IR}				σ_{opt} (6)	Ref. (7)
	$\sigma_{R,unc}$ (2) (km s^{-1})	σ_R (3) (km s^{-1})	R (4) (R_e)	$\sigma_{\pm 7''}$ (5) (km s^{-1})		
N221	70±2	65±2	1/8	70±2	75±3	1, 2
N821	207±5	191±8	1/8	208±5	209±10	3
N1023	216±5	205±6	1/4	217±5	205±10	4
N1068	133±3	133±3	1/8	129±3	151±7	5
N2778	170±4	148±11	1/4	161±4	175±8	3
N2787	188±4	170±4	1	186±3	189±9	6
N3031	166±3	165±4	1/8	157±3	143±7	7
N3115	272±11	236±9	1/8	272±12	230±11	7
N3245	203±5	192±6	1/2	206±7	205±10	7
N3377	148±4	127±3	1/8	147±4	145±7	8, 9
N3379	205±4	205±6	1/8	203±5	206±10	10, 2
N3384	154±3	129±4	1/2	151±3	143±7	3
N3607	210±8	198±7	1/8	210±8	229±11	11
N3608	187±4	193±5	1/8	187±4	182±9	3
N4258	119±3	109±4	1/4	111±2	115±10	6
N4261	290±5	304±8	1/8	286±6	315±15	12, 2
N4291	247±7	245±7	1/4	248±7	242±12	3
N4342	224±5	199±8	1	224±5	225±11	13, 2
N4374	289±7	292±7	1/8	290±8	296±14	14, 2
N4459	157±7	156±7	1/8	164±6	167±8	7
N4473	186±3	173±5	1/2	186±3	190±9	3
N4486	331±11	346±12	1/8	331±11	375±18	15
N4564	177±7	166±6	1/8	175±7	162±8	3
N4596	137±3	136±5	1/2	139±3	136±6	7
N4649	317±11	326±13	1/8	327±11	385±19	3, 15
N4697	174±4	153±4	1/8	172±4	177±8	3
N4742	109±3	86±3	1/4	104±3	90±5	7
N5845	238±4	223±5	1	237±4	234±11	9
N6251	301±11	296±13	1/8	290±8	290±14	17, 2
N7052	365±14	334±15	1/8	327±13	266±13	18
N7457	63±2	60±3	1/8	63±2	67±3	3

NOTE. — Col. (1): Object name. Col. (2): H -band stellar velocity dispersion measured using a single aperture size R without rotation correction. Col. (3): luminosity-weighted H -band σ_* within R . Col. (4): Aperture radius R used for H -band σ_* in units of R_e . Col. (5): H -band velocity dispersion measured using a single aperture within $\pm 7''$. Col. (6): optical stellar velocity dispersions. Col. (7): Reference for optical velocity dispersions.

References. — (1) van der Marel et al. (1998); (2) Gebhardt et al. (2000a); (3) Pinkney et al. (2003); (4) Bower et al. (2001); (5) Nelson & Whittle (1995); (6) Gültekin et al. (2009a); (7) Kormendy & Gebhardt (2001); (8) Kormendy et al. (1998); (9) Gebhardt et al. (2003); (10) Gebhardt et al. (2000b); (11) Gültekin et al. (2009b); (12) van der Marel, Binney & Davies (1990); (13) Cretton & van den Bosch (1999); (14) Bower et al. (1998); (15) Gebhardt et al. (2011); (16) McConnell et al. (2011); (17) Smith, Heckman & Illingworth (1990); (18) van den Bosch & van der Marel (1995)

nificant difference between σ_{opt} and σ_{IR} . The best fit between optical and near-IR measurements is close to a one-to-one relation with a scatter of ~ 0.04 dex (10%) when rotation is not corrected for σ_{IR} . The lower panel in Fig. 8 shows that the rotation-corrected σ_{IR} is slightly smaller than the optical σ_* at lower mass range. However, the average offset is only 7%, which is not significant compared to the measurement uncertainties of stellar velocity dispersions.

Note that McConnell & Ma (2013) included rotation in calculating luminosity-weighted σ_* by adding rotation velocity to velocity dispersion in quadrature (See their Eq. 1). Thus, the slight offset between our σ_{IR} and optical σ_* from McConnell & Ma (2013) may be explained

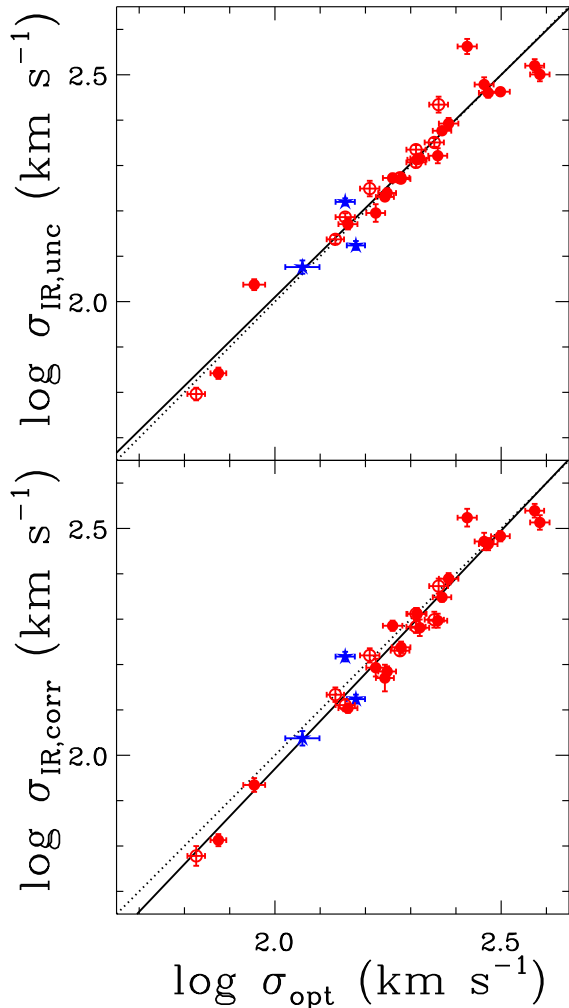


FIG. 8.— Comparison between H -band stellar velocity dispersions and optical stellar velocity dispersions from the literature. H -band σ_* is measured from an extraction aperture, $\pm 7''$ (top panel) or corrected for rotation effect (bottom panel). Elliptical and lenticular galaxies are denoted with filled and open circles while 3 late-type galaxies are indicated by filled stars. The best-fit (solid line) is consistent with a one-to-one relation (dotted line).

by the rotation effect. To test this hypothesis, we derive rotation-included velocity dispersions using the same integral as adopted by McConnell & Ma (2013, Eq. 1). For these consistently measured velocity dispersions, we find that optical and IR velocity dispersions show a one-to-one relationship with a slope of 1.00 ± 0.05 and a 0.03 dex (7%) intrinsic scatter. Thus, we conclude that σ_* measurements derived from optical and H -band stellar lines are consistent.

While many studies have been devoted to measure σ_* of galaxies using optical spectra, the number of σ_* studies based on near-IR data, either H -band or K -band spectra is growing. However, there are currently only few studies that actually compared the results from both wavelength regimes. For example, Silge & Gebhardt (2003) measured σ_* of a sample of 25 elliptical and lenticular galaxies using the $2.29\mu\text{m}$ CO(2-0) band head in the K -band spectra. Comparing their IR results to optical velocity dispersions from the literature, they concluded that IR stellar velocity dispersions can be lower than op-

tical stellar velocity dispersions, by up to 30% – 40% and with a median offset of 11%. The inconsistency between optical and near-IR measurements is probably due to a sample bias and measurement uncertainties. First, their sample mainly consists of S0 galaxies and the systematic difference between optical and near-IR velocity dispersion in their study is mainly caused by S0 galaxies while their elliptical subsample does not show a difference between optical and near-IR measurements. Second, Silge & Gebhardt (2003) measured σ_* using solely a single CO band head in the K -band, which is much more susceptible to template mismatch as explained in their analysis.

In contrast to Silge & Gebhardt (2003), Rothberg & Fischer (2010) reported no inconsistency between optical and near-IR stellar velocity dispersion measurements for elliptical galaxies. Using a sample of 23 elliptical galaxies and 14 merger remnants, they measured σ_* from stellar lines in the K -band spectra, i.e., CO (2-0), CO (3-1), and CO (4-2) band heads, and compare them with velocity dispersion measured from the optical CaII triplet line, showing that optical and near-IR stellar velocity dispersions are virtually the same for elliptical galaxies. For merger remnants Rothberg & Fischer (2010) reported a discrepancy between optical and near-IR velocity dispersions, presumably due to the presence of young stellar population, which are obscured at optical wavelengths. However, for elliptical galaxies, their results indicate that optical and near-IR stellar lines represent the same kinematics and a dust effect is negligible. Similarly, a recent study by Vanderbeke et al. (2011) presented near-IR σ_* measurements also based on the CO band heads for a sample of 22 galaxies, consisting of similar numbers of ellipticals and lenticulars. Comparing with previous optical measurements they reported that optical and near-IR σ_* were consistent for their sample, which is consistent with our results.

In the case of velocity dispersions using H -band stellar lines, there has been no systematic comparison with optical velocity dispersions. Using various stellar lines in the H -band spectra and carefully accounting for the template mismatch problem (see Section 3.2), for the first time, we show that optical and H -band σ_* measurements are consistent for early-type galaxies, indicating that optical and H -band stellar lines represent the same kinematics and that a dust effect, i.e., obscuration at optical wavelengths, is negligible. These results are consistent with K -band stellar kinematics (Rothberg & Fischer 2010; Vanderbeke et al. 2011). Our results imply that near-IR σ_* measurements carried out for AGN host galaxies, for which optical measurements are more difficult to perform due to the strong AGN contribution (e.g., Woo et al. 2010), provide unbiased results, compared to optical measurements.

4.2. The $M_{\text{BH}}-\sigma_*$ Relation for Early-type Galaxies

In this paper we present homogeneously measured σ_* for 31 galaxies with dynamical M_{BH} measurements. By accounting for galaxy rotation and implementing a uniform analysis for measuring velocity dispersions, our σ_* measurements are slightly different from previous optical values. In this section we demonstrate the effect of these new velocity dispersions on the $M_{\text{BH}}-\sigma_*$ relation by fit-

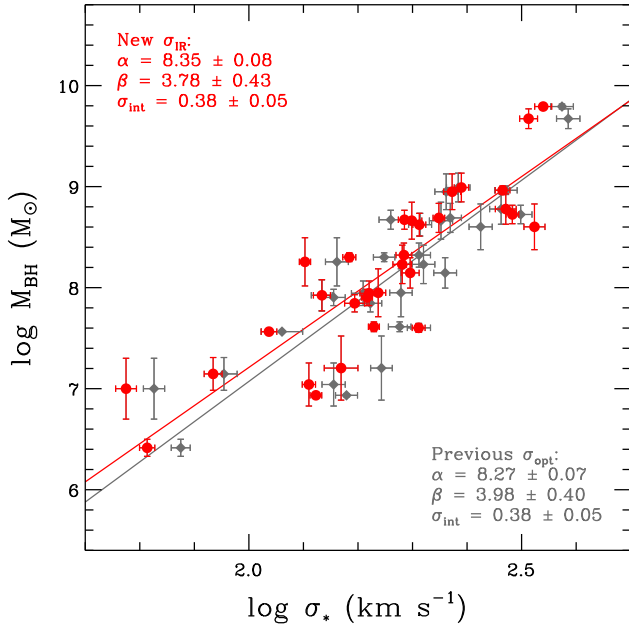


FIG. 9.— The $M_{\text{BH}}-\sigma_*$ relation of 31 nearby galaxies, using rotation-corrected σ_* measured from our H-band spectra (red circles, red line) and rotation-included optical σ_* from McConnell & Ma (2013) (gray diamonds, gray line), respectively.

ting the $M_{\text{BH}}-\sigma_*$ relation for 31 galaxies, for which we obtained the rotation-corrected σ_* . Results on the $M_{\text{BH}}-\sigma_*$ relation for the full sample of galaxies with dynamical M_{BH} will be presented in a companion paper (Woo et al. 2013 in preparation). For this analysis, we used the most recent M_{BH} updates from McConnell & Ma (2013).

We fit the $M_{\text{BH}}-\sigma_*$ relation as a single-index power law:

$$\log(M_{\text{BH}}/M_{\odot}) = \alpha + \beta \log(\sigma_*/200 \text{ km s}^{-1}). \quad (2)$$

We used the FITEXY method, modified to account for intrinsic scatter in the relation (Tremaine et al. 2002; Park et al. 2012), to perform the fit as shown in Figure 9.

By fitting the $M_{\text{BH}}-\sigma_*$ relation using the optical σ_* from McConnell & Ma (2013), we obtain $\alpha = 8.27 \pm 0.07$, $\beta = 3.98 \pm 0.40$ and an intrinsic scatter of 0.38 ± 0.05 dex. Our sample has a large overlap with the sample used by Tremaine et al. (2002), and indeed we obtain consistent results for the $M_{\text{BH}}-\sigma_*$ relation. The slight difference arises mainly from a few different galaxies in both samples and from updated M_{BH} determinations (e.g. Schulze & Gebhardt 2011). By fitting the $M_{\text{BH}}-\sigma_*$ relation using our rotation-corrected near-IR σ_* , we find $\alpha = 8.35 \pm 0.08$, $\beta = 3.78 \pm 0.43$ and an intrinsic scatter of 0.38 ± 0.05 dex. This relation is slightly shallower than that derived from optical σ_* , but consistent within the uncertainties.

Note that the previous studies on the $M_{\text{BH}}-\sigma_*$ relation by Gültekin et al. (2009a) and McConnell & Ma (2013) explicitly included rotation in calculating luminosity-weighted σ_* . In this case, we expect systematic effect on the measured σ_* due to the random orientation of stellar disk with respect to the line-of-sight. To investigate this effect, we calculated σ_* by adding velocity to velocity dispersion in quadrature using Eq. 1 in McConnell & Ma (2013). The result shows that rotation-included σ_* is

slightly larger than rotation-corrected σ_* , particularly at low mass scale, by 0.02 dex ($\sim 5\%$) on average with a 0.02 ($\sim 5\%$) scatter. Consequently, when we replace rotation-corrected σ_* with rotation-included σ_* in fitting the $M_{\text{BH}}-\sigma_*$ relation, the slope slightly increases from 3.78 ± 0.43 to 3.97 ± 0.49 as the σ_* values increase preferentially at low mass scale, while intrinsic scatter remains the same.

Although we expect that the rotation effect will systematically affect the $M_{\text{BH}}-\sigma_*$ relation, we do not clearly detect the improvement of the $M_{\text{BH}}-\sigma_*$ relation by using rotation-corrected σ_* , presumably due to two reasons. First, rotation effect on the luminosity-weighted velocity dispersion may not be significant as the integrated velocity dispersions are dominated by the inner part, where the rotation velocity is relatively small. In the case of the rotation-included velocity dispersion, the luminosity weight of the inner part is more dominant since velocity dispersions are integrated in quadrature (see Eq. 1 in McConnell & Ma 2013). Secondly, since our sample is mainly composed of early-type galaxies, rotation effect is relatively weak compared to late-type galaxies. For late-type galaxies with a low σ_* , rotation effect can be significant, hence, it would be essential to correct for, in order to properly derive the $M_{\text{BH}}-\sigma_*$ relation.

For massive BHs, the sphere of influence of BH can be large enough to change the effective σ_* measurements since the velocity dispersion at the center increases due to the presence of a BH. Thus, by excluding the sphere of influence of BH in calculating the luminosity-weighted σ_* , the effective velocity dispersions will be decreased. Since these corrections can be done only for massive galaxies with a resolved sphere of influence, the slope of the $M_{\text{BH}}-\sigma_*$ relation will increase due to the preferential decrease of σ_* at high mass end. For example, by excluding the sphere of influence of BH in deriving the effective σ_* within R_e for 12 most massive galaxies, McConnell & Ma (2013) showed that the slope of the $M_{\text{BH}}-\sigma_*$ relation increased from 5.48 ± 0.30 to 5.64 ± 0.32 . We performed a similar analysis using our data although only two galaxies, NGC 4486 and NGC 4649, are among those 12 galaxies with a resolved sphere of influence. By excluding the sphere of influence of BH, the luminosity-weighted σ_* decreases from 346 ± 12 to 327 ± 11 for NGC 4486, and from 346 ± 12 to 327 ± 11 for NGC 4649. Based on these two updated σ_* , the slope of the $M_{\text{BH}}-\sigma_*$ relation slightly increases from 3.78 ± 0.43 to 3.79 ± 0.45 , however two slopes are consistent within the uncertainties. Using only 2 galaxies, it is not clear whether excluding or including the sphere of influence in determining the effective σ_* improves the $M_{\text{BH}}-\sigma_*$ relation.

Compared to the $M_{\text{BH}}-\sigma_*$ relation recently presented by McConnell & Ma (2013), we find a significantly shallower slope. They report a slope of 5.64 ± 0.32 , using a much larger galaxy sample, which includes in particular more galaxies at higher and lower masses. We will investigate the implications of our results on the $M_{\text{BH}}-\sigma_*$ relation in detail in a companion paper (Woo et al. 2013 in preparation).

5. SUMMARY

We observed a sample of 31 nearby galaxies with Triplespec, a near-IR long-slit spectrograph at the Palomar 5-m telescope in order to homogeneously measure

velocity dispersions from the H -band stellar lines. The galaxies in the sample cover a wide range in σ_* ($67 \text{ km s}^{-1} < \sigma_* < 385 \text{ km s}^{-1}$) and their dynamical central BH masses are also available. To account for template mismatch, we used 11 giant stars with spectral type ranging from K0 to M5 as velocity templates, and found that M giants generate the most reliable fits and velocity dispersion measurements.

By measuring velocity and velocity dispersion as a function of radius along the major axis of each galaxy, we determined the rotation curve and velocity dispersion profile. Using these spatially resolved velocity dispersion measurements, we calculated the luminosity-weighted stellar velocity dispersions within the R_e of each galaxy. For 25 out of 31 galaxies in the sample, we found a clear rotation component, indicating that stellar velocity dispersions can be significantly overestimated due to the rotational broadening if a large single aperture is used to extract spectra. Compared to rotation-corrected velocity dispersions, velocity dispersions measured from single-aperture spectra showed systematically larger values by up to $\sim 20\%$.

We compared velocity dispersions measured from H -band stellar lines with those measured from optical lines and found no systematic difference, suggesting that optical and H -band stellar lines represent the same kinematics and that dust effect is negligible for early-type galaxies. Our results confirm that optical and near-IR

stellar lines can be interchangeably used to measure stellar kinematics and near-IR σ_* measured for AGN host galaxies can be directly compared to optical σ_* of quiescent galaxies.

Using the rotation-corrected σ_* measurements based on the spatially-resolved H -band spectra of 31 nearby galaxies, we derived the $M_{\text{BH}}-\sigma_*$ relation to investigate rotation effect. The slope of the $M_{\text{BH}}-\sigma_*$ relation is slightly shallower than that based on the rotation-included optical or near-IR σ_* measurements. Although rotation effect is not dramatically strong for early-type galaxies, it is potentially important to correct for, particularly for low mass, late-type galaxies with a strong rotation component, in order to properly determine the $M_{\text{BH}}-\sigma_*$ relation and its intrinsic scatter. A future study based on spatially resolved spectra for late-type galaxies is required to fully quantify rotation effect on the $M_{\text{BH}}-\sigma_*$ relation.

We thank the anonymous referee for constructive suggestions, which improved the manuscript. This work was supported by the National Research Foundation of Korea (NRF) grant funded by the Korea government (MEST) (No. 2012-006087). J.H.W acknowledges the support by the Korea Astronomy and Space Science Institute (KASI) grant funded by the Korea government (MEST).

REFERENCES

- Barth, A. J., et al. 2001, ApJ, 555, 685
 Bender, R., Saglia, R. P., & Gerhard, O. E. 1994, MNRAS, 269, 785
 Bennert, V. N., Treu, T., Woo, J.-H., et al. 2010, ApJ, 708, 1507
 Bennert, V. N., et al. 2011a, ApJ, 726, 59
 Bennert, V. N., Auger, M. W., Treu, T., Woo, J.-H., & Malkan, M. A. 2011b, ApJ, 742, 107
 Bower, G. A., et al. 1998, ApJ, 492, L111
 Bower, G. A., et al. 2001, ApJ, 550, 75
 Cretton, N., & van den Bosch, F. C. 1999, ApJ, 514, 704
 Dasra, K. M., et al. 2007, ApJ, 657, 102
 Devereux, N., Ford, H., Tsvetanov, Z., & Jacoby, G. 2003, AJ, 125, 1226
 Dressler A. 1984, ApJ, 286, 97
 Emsellem, E., Dejonghe, H., & Bacon, R. 1999, MNRAS, 303, 495
 Ferrarese, L., & Ford, H. C. 1999, ApJ, 515, 583
 Ferrarese, L., & Ford, H. 2005, Space Sci. Rev., 116, 523
 Ferrarese, L., Ford, H., & Jaffe, W. 1996, ApJ, 470, 444
 Ferrarese, L., & Merritt, D. 2000, ApJ, 539, L9
 Gebhardt, K., et al. 2000a, ApJ, 539, L13
 Gebhardt, K., et al. 2000b, AJ, 119, 1157
 Gebhardt, K., et al. 2003, ApJ, 583, 92
 Gebhardt, K., et al. 2011, ApJ, 729, 119
 Graham, A. W. 2008, ApJ, 680, 143
 Gültekin, K., et al. 2009a, ApJ, 698, 198
 Gültekin, K., et al. 2009b, ApJ, 695, 1577
 Harris, C. E., Bennert, V. N., Auger, M. W., et al. 2012, ApJS, 201, 29
 Herrnstein, J. R., Moran, J. M., Greenhill, L. J., & Trotter, A. S. 2005, ApJ, 629, 719
 Kent S. M. 1990, AJ, 100, 377
 Kormendy, J., Bender, R., Evans, A., & Richstone, D. 1998, AJ, 115, 1823
 Kormendy, J., & Gebhardt, K. 2001, in AIP Conf. Ser. 586, 20th Texas Symposium on Relativistic Astrophysics, ed. J. C. Wheeler & H. Martel (Melville, NY: AIP), 363
 Lodato, G., & Bertin, G. 2003, A&A, 398, 517
 Marconi, A., & Hunt, L. K. 2003, ApJ, 589, L21
 McConnell, N. J., et al. 2011, Nature, 480, 215
 McConnell, N. J., Ma, C.-P., Murphy, J. D., et al. 2012, ApJ, 756, 179
 McConnell, N. J., & Ma, C.-P. 2013, ApJ, 764, 184
 Nelson, C. H., & Whittle, M. 1995, ApJS, 99, 67
 Onken, C. A., et al. 2004, ApJ, 615, 645
 Park, D., Kelly, B. C., Woo, J.-H., & Treu, T. 2012, ApJS, 203, 6
 Pinkney, J., et al. 2003, ApJ, 596, 903
 Rothberg, B., & Fischer, J. 2010, ApJ, 712, 318
 Sani, E., Marconi, A., Hunt, L. K., & Risaliti, G. 2011, MNRAS, 413, 1479
 Sarzi, M., et al. 2001, ApJ, 550, 65
 Schulze, A., & Gebhardt, K. 2011, ApJ, 729, 21
 Shen, J., & Gebhardt, K. 2010, ApJ, 711, 484
 Silge, J. D., & Gebhardt, K. 2003, AJ, 125, 2809
 Smith, E. P., Heckman, T.M., & Illingworth, G. D. 1990, ApJ, 356, 399
 Tremaine, S., et al. 2002, ApJ, 574, 740
 van den Bosch, F. C., & van der Marel, R. P. 1995, MNRAS, 274, 884
 van den Bosch R. C. E., & de Zeeuw, P. T. 2010, MNRAS, 401, 1770
 Vanderbeke, J., Baes, M., Romanowsky, A. J., & Schmidtbreick, L. 2011, MNRAS, 412, 2017
 van der Marel, R. P. 1994, MNRAS, 270, 271
 van der Marel, R. P., Cretton, N., de Zeeuw, P. T., & Rix, H.-W. 1998, ApJ, 493, 613
 van der Marel, R. P., & van den Bosch, F. C. 1998, ApJ, 116, 2220
 van der Marel, R. P., Binney, J., & Davies, R. L. 1990, MNRAS, 245, 582
 Verolme E. K., et al. 2002, MNRAS, 335, 517
 Walsh, J. L., Barth, A. J., & Sarzi, M. 2010, ApJ, 721, 762
 Watson, L. C., et al. 2008, ApJ, 682, L21
 Woo, J.-H., Urry, C. M., Lira, P., van der Marel, R. P., & Maza, J. 2004, ApJ, 617, 903
 Woo, J.-H., Urry, C. M., van der Marel, R. P., Lira, P., & Maza, J. 2005, ApJ, 631, 762
 Woo, J.-H., Teru, T., Malkan, M. A., & Blandford, R. D. 2006, ApJ, 645, 900
 Woo, J.-H., Treu, T., Malkan, M. A., & Blandford, R. D. 2008, ApJ, 681, 925
 Woo, J.-H., et al. 2010, ApJ, 716, 269